RESEARCH ARTICLE

Journal of Medical Imaging and Health Informatics
Vol. 7, 890–896, 2017

Synchrotron Radiation Imaging of Aortic Stent Grafting: An *In Vitro* Phantom Study

Zhonghua Sun* and Curtise K. C. Ng

Department of Medical Radiation Sciences, Curtin University, Perth, Western Australia, 6845, Australia

This study was conducted on a human aorta phantom with a commercially available stent graft placed in the aorta with the aim of investigating visualization of aortic stent graft by synchrotron radiation. Synchrotron tomography experiments were performed on imaging and medical beamline at the Australian Synchrotron facility, with beam energy ranging from 40 to 100 keV, with spatial resolution of 19.88 μm per pixel. Computed tomography (CT) scans were performed on a 64-slice CT scanner with slice thickness of 1.0, 1.5 and 2.0 mm. Maximal transverse diameter of stent wires was measured on synchrotron radiation and 64-slice CT images at suprarenal stent struts and main body of aortic stent graft. The stent wire diameter measured on synchrotron images was between 0.4 and 0.5 mm, representing the actual diameter of wire thickness, while overestimated wire thickness was seen in 64-slice CT images with measured wire diameter ranging from 1.0 to 1.6 mm. There were no significant differences in stent wire diameter between suprarenal stent struts and main body stent graft by comparing two-dimensional (2D) axial ($p = 0.93$) and three-dimensional (3D) synchrotron image measurements ($p = 0.07$). Significant difference was found between 2D and 3D synchrotron measurements of stent wire diameter in the main body of stent graft ($p = 0.001$). In contrast, significant differences were found in stent wire diameter at the levels of suprarenal stent struts and the main body of stent graft by comparing 2D axial and 3D CT image measurements ($p = 0.03$ and 0.001 respectively). Also, significant differences were reached by comparing measurements taken at the suprarenal stent struts and main body of stent graft with use of 2D axial ($p = 0.04$) and 3D CT images ($p = 0.001$). Synchrotron radiation provides superior advantages over multislice CT for visualization of aortic stent wire structure with measurements representing the actual diameter, thus allowing accurate assessment of endovascular stent graft repair.

Keywords: Aortic Stent Graft, Phantom, Synchrotron Radiation, Stent Wire, 3D Visualization.

1. INTRODUCTION

Endovascular aneurysm repair (EVAR) of abdominal aortic aneurysm (AAA) has become a widely performed procedure to treat patients with AAA due to its less invasiveness and associated low peri-operative mortality when compared to open surgery.[1–5] Technical developments in aortic stent grafts have extended the application of EVAR to benefit more patients with complicated aortic aneurysmal diseases, with resultant modifications in stent graft design ranging from traditional infrarenal aortic stent grafts to suprarenal and fenestrated stent grafts.[6–11] Although promising results have been reported in many studies with use of EVAR for treatment of patients with AAA, the long-term outcomes, in particular the effect of stent wires on subsequent renal function remain to be determined.[6, 12–15]

Currently, computed tomography (CT) angiography is the preferred imaging modality for both preoperative planning and postprocedural follow-up of EVAR.[16–20] Despite rapid developments in multislice CT scanners with high spatial resolution leading to isotropic voxel size of $0.4 \times 0.4 \times 0.4$ mm^3,[3, 21–23] stent wire diameter is often overestimated on CT images due to point spread function of CT imaging, which results in wire thickness between 1.0 and 2.0 mm, while the actual diameter of aortic stent wires is less than 0.5 mm.[24–26] This is clinically important in patients treated with suprarenal stent grafts since there exists potential interference with renal blood perfusion by stent wires.[27–29] Therefore, reliable assessment of aortic stent wires by a high resolution imaging technique is of paramount importance to ensure safe implantation of stent grafts, and this could be achieved with synchrotron radiation imaging.

Synchrotron imaging represents an immense leap forward in performance over imaging techniques with use of conventional X-ray sources due to its superior resolution (10–20 μm as opposed to the 300–400 μm with currently available multislice CT scanners) and has been extensively exploited in many areas of science including medical applications.[30] Promising results of using synchrotron radiation in the investigation of cardiovascular disease have been reported in the literature.[31–33] In these studies, researchers were able to quantitatively assess the restenosis in stents and human atherosclerotic plaques. The actual structure

*Author to whom correspondence should be addressed.

 2156-7018/2017/7/890/007 doi:10.1166/jmihi.2017.2094

of real human plaques and the chemical composition of calcified lesions could be revealed with synchrotron imaging. Further, the mechanical structure of the coronary stent was clearly imaged and visualized. With its high spatial resolution and low radiation dose, synchrotron radiation could be a potential imaging technique to accurately evaluate the suprarenal stent wires in relation to the renal artery ostium. The aim of this study is to investigate the application of synchrotron radiation in imaging aortic stent graft based on an *in vitro* phantom study. We hypothesized that synchrotron radiation allows for more accurate assessment of aortic stent wires in comparison with conventional CT imaging.

2. MATERIALS AND METHODS

2.1. Human Aorta Phantom

This is an *in vitro* phantom study with use of a human aorta model consisting of the aneurysm, superior mesenteric artery and renal arteries (Fig. 1). The aorta model was built with medical rapid prototyping technique based on our previous studies, and it represents the accuracy of actual diameters of the aorta and its main branches.[24–26]

2.2. Aortic Stent Graft

In order to simulate endovascular aortic repair, a commercially available Zenith AAA endovascular stent graft (William Cook Europe, Bjaeverskov, Denmark) was used as it has an uncovered suprarenal component consisting of bare metal stent wires which allow blood perfusion to the kidneys once the stent graft is placed across the renal arteries. Figure 2 shows the Zenith stent graft with suprarenal stent wires. The suprarenal stent wire was measured 0.47 mm while the stent wire in the main body of stent graft was measured 0.46 mm.

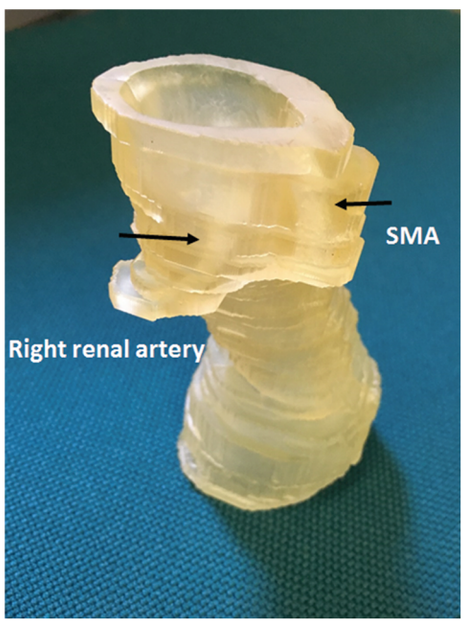

Fig. 1. Human aorta phantom manufactured by rapid prototyping technique showing superior mesenteric and renal arteries (arrows). SMA-superior mesenteric artery.

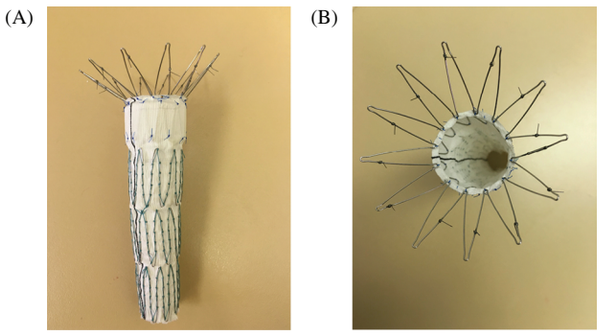

Fig. 2. Zenith AAA stent graft. (A) Lateral view of stent graft with an uncovered suprarenal component. (B) Top view of suprarenal stent wires with hooks and barbs.

2.3. Synchrotron Radiation Experimental Set-Up

The synchrotron tomography experiments were performed on imaging and medical beamline (IMBL) at the Australian Synchrotron Facility in Melbourne, Australia. This is a method of imaging that utilises single energy X-rays from a synchrotron source and has produced images of test objects and tissues whose contrast and information content far exceed conventional imaging techniques.[32, 33]

For tomography imaging, a parallel beam of monochromatic X-ray was used with a single two-dimensional (2D) detector behind the sample for data collection. The sample was rotated to acquire the projection images for tomographic reconstruction. Projections were taken every 0.1° for a total sample rotation of 180°, giving 1800 projections per scan. Reconstruction using a filtered back projection algorithm was performed off-line on a workstation. Images were recorded on detectors with a field of view 70 mm by 20 mm with pixel size 19.88 μm.

Once the aorta phantom was secured and aligned properly (Fig. 3), a range of beam energies was tested from 40 to 100 keV

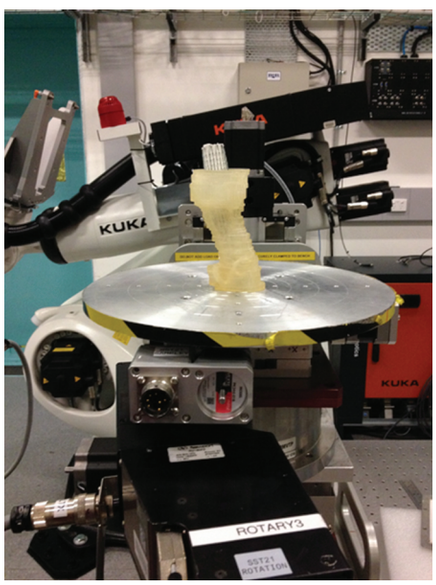

Fig. 3. Experimental set-up of synchrotron radiation of aortic phantom study. The phantom with aortic stent graft in place is positioned at the center of beam line.

with an increment of 10 keV at each step with the aim of determining the effects of different beam energies on the visualization of stent wires. The beam energy of 50 keV was not included in the scanning protocol because we first tested the lowest levels of 40 and 50 keV and noticed that both energy levels did not show the stent wires clearly, thus, only 40 keV was used as the lowest beam energy level.

2.4. CT Scanning Protocols

CT scans were performed on a 64-slice CT scanner (Siemens Definition, Siemens Healthcare, Forchheim, Germany) with the following scanning protocol: beam collimation $2 \times 32 \times 0.6$ mm, kVp 100, tube current 180 mA, slice thickness ranging from 1.0, 1.5 and 2.0 mm with 50% reconstruction interval with pitch of 1.5. Selection of these protocols was based on our previous study with regard to optimizing image quality and radiation dose in aortic stent grafting. The effective radiation dose associated with these CT scanning protocols was between 1.88 and 2.04 mSv according to our previous study.[34]

2.5. Image Processing and Data Measurements

Original 2D axial synchrotron images in tagged image file format (TIFF) and 64-slice CT images in Digital Imaging and Communications in Medicine (DICOM) format were processed with the commercial software, Analyze V 12.0 (AnalyzeDirect, Inc., Lexana, KS, USA). Data were transferred to a separate workstation equipped with this software for image processing and measurement. Measurements of stent wire diameter at maximal transverse dimensions were performed on both 2D axial and three-dimensional (3D) volume rendering images acquired with 64-slice CT and synchrotron radiation imaging respectively. Measurements were taken at five different locations at the levels of suprarenal stent struts and main body of stent graft, with the mean value taken as final to avoid intra-observer bias. Measurements were performed by an experienced radiologist who has more than 15 years of experience in stent graft imaging.

2.6. Statistical Analysis

Statistical analyses were performed using SPSS 24.0 (SPSS Inc, Chicago., IL, USA). Continuous variables were expressed as the mean ± standard deviation. A student t test was used to compare the differences between measured wire thicknesses based on synchrotron radiation and multislice CT images. A p value less than 0.05 was considered statistically significant.

3. RESULTS

A total of 9 datasets were acquired for analysis with 6 from synchrotron radiation and 3 from 64-slice CT imaging. Table I shows results of measuring stent wire thickness at suprarenal stent struts and main body of stent graft locations.

Results of synchrotron tomography imaging showed that the measured sizes of suprarenal stent wires were very close to the actual wire thickness between 0.4 and 0.5 mm. The exposure protocol of 40 keV resulted in the largest wire diameter with visualization of stent wires affected to some extent due to insufficient exposure as shown in Figure 4. When the beam energy was gradually increased from 40 to 100 keV, stent wires became clearly visualized on both 2D axial and 3D reconstruction images (Figs. 5 and 6). Although the measured wire thickness decreased with the increase of keV on 2D and 3D images, there were no significant differences in stent wire diameter measured with 2D axial and 3D images at the level of suprarenal stent struts ($p = 0.09$). Similarly, no significant differences were found in stent wire diameter between suprarenal stent struts and main body of stent graft by comparing 2D axial ($p = 0.93$) and 3D image measurements ($p = 0.07$). The only significant difference was found between 2D axial and 3D image measurements in the main body of stent graft, with wire thickness measured on 3D images significantly smaller than that on 2D images ($p = 0.001$).

Table I. Measurements of stent wire diameters at different regions of aortic stent graft.

	Suprarenal stent struts (mm) (mean ± SD)		Main body of stent graft (mm) (mean ± SD)	
Imaging parameters	2D axial images	3D images	2D axial images	3D images
Synchrotron imaging (keV)				
40	0.52 ± 0.02	0.45 ± 0.01	0.51 ± 0.01	0.40 ± 0.01
60	0.46 ± 0.01	0.43 ± 0.03	0.46 ± 0.01	0.36 ± 0.01
70	0.42 ± 0.02	0.39 ± 0.02	0.42 ± 0.01	0.34 ± 0.01
80	0.42 ± 0.01	0.37 ± 0.01	0.42 ± 0.01	0.33 ± 0.01
90	0.40 ± 0.01	0.35 ± 0.01	0.40 ± 0.01	0.32 ± 0.01
100	0.40 ± 0.01	0.33 ± 0.01	0.42 ± 0.01	0.29 ± 0.01
64-slice CT imaging (mm)				
1.0	1.49 ± 0.10	1.32 ± 0.11	1.32 ± 0.18	0.95 ± 0.05
1.5	1.63 ± 0.06	1.44 ± 0.11	1.40 ± 0.08	1.03 ± 0.13
2.0	1.62 ± 0.14	1.42 ± 0.10	1.47 ± 0.11	1.03 ± 0.09

Note: 2D = 2-dimensional; 3D = 3-dimensional; CT = computed tomography; SD = standard deviation.

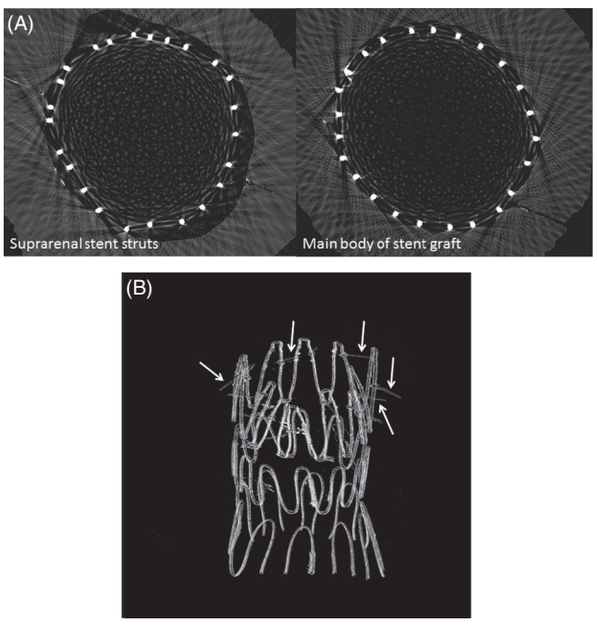

Fig. 4. Synchrotron tomography images acquired with 40 keV beam energy. (A) 2D axial images show suprarenal stent wires and main body of stent graft. (B) 3D reconstructed image indicates suboptimal visualization of stent wires due to insufficient energy resulting in artefacts.

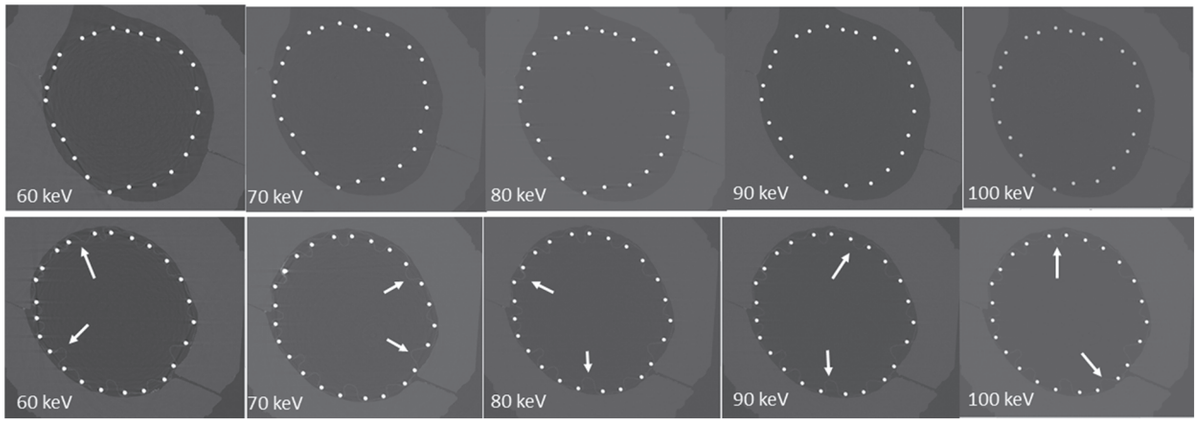

Fig. 5. Synchrotron tomography images acquired with beam energy ranging from 60 to 100 keV. 2D axial images of suprarenal stent struts (top row) and main body of stent graft (bottom row). Arrows refer to the stent graft material.

Results of 64-slice CT images showed overestimated wire thickness with use of different slice thicknesses, with wire diameter 2–3 fold of the actual size. Stent wires appear to be larger with the increase of slice thickness as shown in Table I. Significant differences were found in stent wire diameter at the levels of suprarenal stent struts and the main body of stent graft by comparing 2D axial and 3D image measurements ($p = 0.03$ and 0.001 respectively). Also, significant differences were reached by comparing measurements taken at the suprarenal stent struts and main body of stent graft with use of 2D axial ($p = 0.04$) and 3D images ($p = 0.001$). Figure 7 shows 2D axial images acquired with different CT protocols, while Figure 8 is an example showing 3D reconstructions of aortic stent graft.

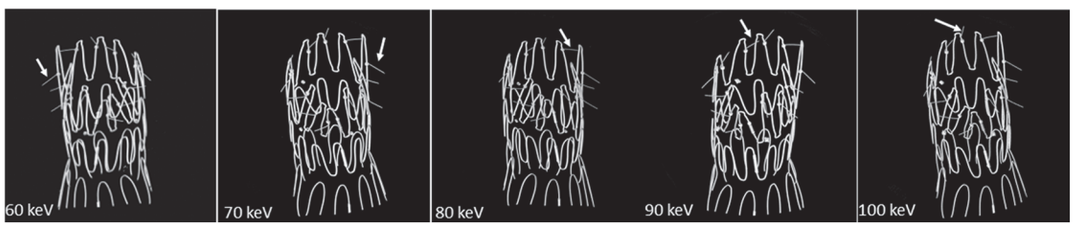

Fig. 6. Synchrotron tomography images acquired with beam energy ranging from 60 to 100 keV. 3D reconstructed images demonstrate stent wires clearly with fine details visualized at the suprarenal stent struts with wire thickness similar to the actual diameter. Arrows point to the hooks at the suprarenal stent wires.

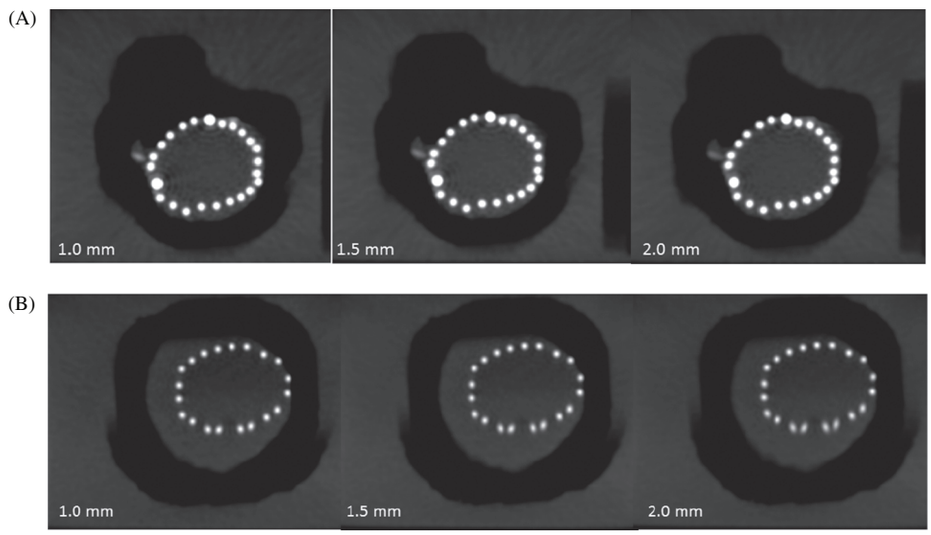

Fig. 7. 64-slice CT 2D views of aortic stent graft. 2D axial images showing suprarenal stent struts (A) and main body of stent graft (B).

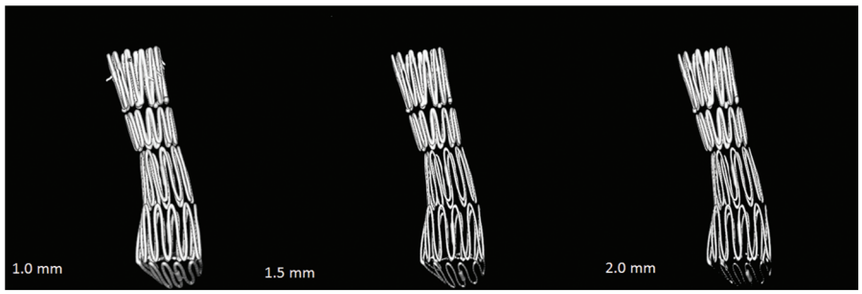

Fig. 8. 64-slice CT 3D views of aortic stent graft. 3D reconstructed images showing aortic stent graft with wire thickness overestimated greatly when compared to synchrotron images as demonstrated in Figure 6.

4. DISCUSSION

This study was designed to investigate the application of synchrotron radiation in the assessment of aortic stent grafting with a focus on the visualization of stent wires and measurement of wire thickness in comparison with 64-slice CT scanning. Results of this study showed the superiority of synchrotron radiation with stent wires clearly visualized on 2D axial and 3D reconstructed images. Further, fine details of aortic stent graft such as barbs of hooks (Fig. 6) comprising the suprarenal component can also be demonstrated on the synchrotron images as compared to CT images. Thus, synchrotron radiation allows for more accurate assessment of stent graft structures.

The rationale behind this study is to utilize the recently established synchrotron facility in Australia and provide new insight into the anatomical structure of endovascular aortic stent grafts, for advancing our understanding of the endovascular repair of AAA that will contribute to improvements in the long-term safety of this surgical procedure. The renal artery ostium normally ranges from 5 to 7 mm in diameter, whereas the thickness of stent struts is about 0.4–0.5 mm. CT image findings of this study are consistent with our previous reports showing that suprarenal stent struts were overestimated with measured wire thickness ranging from 1.0 mm to 1.6 mm in diameter on 2D and 3D visualizations.[24–26] This prevents accurate assessment of the encroachment of stent wires to the renal artery ostium. Thus, an imaging modality to overcome the above limitations inherent in CT imaging is important for clinicians to evaluate the treatment outcomes of EVAR. We believe synchrotron imaging holds promise as such a method, and this is confirmed by findings presented in this study with measured wire diameter similar to the actual diameter.

The synchrotron radiation facility produces high intensity light beams across multiple wavelengths. The unique features of synchrotron light make research results far superior in accuracy, clarity and specificity than with conventional medical imaging modalities. The advantages of synchrotron radiation imaging have been increasingly explored in medical applications such as 3D morphology of cell structures,[35] micro-architectural alterations in osteoarthritis and cartilage,[36,37] biological morphology and biomaterial science.[38] In the diagnosis of cardiovascular disease, synchrotron radiation has been shown to allow accurate characterization of atherosclerotic plaques both qualitatively and quantitatively with excellent correlation to histopathologic findings.[39,40] With more than 10-fold resolution of current CT scanners, this study shows synchrotron radiation enables detection of not only stent wire structures, but also other fine details associated with stent graft such as barbs and hooks, as shown in the results of this study. Thus, research findings offer insights into accurate assessment and characterization of aortic stent wire details.

Although it is unrealistic to use synchrotron imaging for routine follow-up of patients treated with endovascular stent grafts, synchrotron radiation angiography has been proved to be a novel and safe tool for imaging of cardiovascular disease in patients.[41] This study provides a scientific basis on management of patients who develop post-procedural complications which cannot be resolved with conventional CT imaging. Therefore, phantom-based experiments using synchrotron radiation will play a significant role in improving understanding of the treatment effects of the EVAR and identification and characterization of problems related to the stent grafting.

Some limitations in this study should be acknowledged. First, although Zenith stent graft was placed in the aorta phantom to simulate treatment of AAA, there was no contrast medium used to represent routine CT angiographic scans due to its potential interference of contrast medium with stent wire visualization. Second, we did not analyse the effect of stent wires in relation to the renal artery ostium as the focus of this study is to compare the stent wire thickness measured with various beam energies from synchrotron radiation and different slice thicknesses from 64-slice CT. Further studies are necessary to quantify this effect. Third, the 64-slice CT scanner used in this study is a widely available multislice CT scanner in clinical centers. Although latest scanners including 320-slice and 3rd generation dual-source CT represent the most recent CT models which offer longer z-axis anatomical coverage and improved temporal resolution, there is no difference in spatial resolution to that of 64-slice CT.[23] Thus, images acquired with the 64-slice CT in this study are not inferior to those with latest CT scanners. Finally, although the current aorta phantom represents anatomical details of human aorta and aortic aneurysm, patient-specific realistic 3D printed models could be used for further experiments. 3D printed models based on individual patient's medical images such as echocardiographic, computed tomographic or magnetic resonance imaging have been shown to guide pre-surgical simulation and planning, and intraoperative orientation through providing unique anatomy for individual patients diagnosed with complex cardiovascular disease.[42–44] Further, only one type of stent graft (Zenith suprarenal stent graft) was included in this study. Due to increasing use of different types of stent grafts for treatment of AAA,[8–12] further research with inclusion of more stent grafts such as fenestrated stent grafts is necessary to verify the results as shown in this study.

In conclusion, in this phantom study we demonstrate the advantage of synchrotron radiation over multislice CT imaging in the visualization of aortic stent graft. Aortic stent wires are clearly visualized on synchrotron images with wire thickness representing the actual diameter when beam energy of 60 keV or higher is applied. The high-resolution images acquired with synchrotron radiation are able to demonstrate anatomical details of aortic stent graft. This technique could be a potential imaging modality for more accurate assessment of encroachment of stent wires to the renal artery ostium although this needs to be verified by further studies.

Acknowledgments: Authors would like to thank Dr. Chris Hall from Australian Synchrotron for his advice and assistance in our experiments.

References and Notes

1. R. M. Greenhalgh, L. C. Brown, G. P. Kwong, J. T. Powell, and S. G. Thompson, EVAR trial participants. Comparison of endovascular aneurysm repair with open repair in patients with abdominal aortic aneurysm (EVAR trial1), 30-day operative mortality results: Randomised controlled trial. *Lancet*. 364, 843 **(2004)**.
2. M. Prinssen, E. L. Verhoeven, J. Buth, P. W. Cuypers, M. R. van Sambeek, R. Balm, E. Buskens, D. E. Grobbee, and J. D. Blankensteijn, Dutch Randomized Endovascular Aneurysm Management (DREAM) Trial Group. A randomized trial comparing conventional and endovascular repair of abdominal aortic aneurysms. *N. Engl. J. Med*. 351, 1607 **(2004)**.
3. P. L. Harris, S. R. Vallabhaneni, O. Desgranges, J. P. Becquemin, C. van Marrewijk, and R. J. Laheij. Incidence and risk factors or late rupture, conversion and death after endovascular repair of infrarenal aortic aneurysm: The EUROSTAR experience. European Collaboration on Stent/graft techniques for aortic aneurysm repair. *J. Vasc. Surg.* 32, 739 **(2000)**.
4. EVAR Trial Participants, Endovascular aneurysm repair and outcome in patients unfit for open repair of abdominal aortic aneurysm (EVAR trial 2): Randomised controlled trial. *Lancet,* 365, 2187 **(2004)**.
5. L. C. Brown, R. M. Greenhalgh, S. G. Thompson, and J. T. Powell, on behalf of The EVAR Trial Participants. Does EVAR alter the rate of cardiovascular events in patients with abdominal aortic aneurysm considered unfit for open repair: Results from the randomized EVAR Trial 2. *Eur. J. Vasc. Endovasc. Surg.* 39, 396 **(2010)**.
6. M. O'Donnell, Z. Sun, J. Winder J, P. K. Ellis, L. L. Lau, and P. H. Blair. Suprarenal fixation of endovascular aortic stent grafts: Assessment of medium-term to long-term renal function by analysis of juxtarenal stent morphology. *J. Vasc. Surg.* 45, 694 **(2007)**.
7. R. K. Greenberg, T. A. Chuter, M. Lawrence-Brown, S. Haulon, and L. Nolte; Zenith Investigators, Analysis of renal function after aneurysm repair with a device using suprarenal fixation (Zenith AAA Endovascular Graft) in contrast to open surgical repair. *J. Vasc. Surg.* 39, 1219 **(2004)**.
8. B. E. Muhs, E. L. Verhoeven, C. Zeebregts, I. F. Tielliu, T. R. Prins, H. J. M. Verhagen, and J. A. M. V. D. Dungen, Mid-term results of endovascular aneurysm repair with branched and fenestrated endografts. *J. Vasc. Surg.* 44, 9 **(2006)**.
9. E. L. G. Verhoeven, T. R. Prins, I. F. J. Tielliu, C. A. J. M Zeebregts, R. G. Hulsebos, V. A. D. Kempenaer, M. Oudkerk, and R. V. Schifgaarde, Treatment of short-necked infrarenal aortic aneurysms with fenestrated stent-grafts: Short-term results. *Eur. J. Vasc. Endovasc. Surg.* 27, 477 **(2004)**.
10. C. D. Bicknell, N. J. Cheshire, C. V. Riga, P. Bourke, J. H. Wolfe, R. G. J. Gibbsm, M. P. Jenkins, and M. Hamady, Treatment of complex aneurysmal disease with fenestrated and branched stent grafts. *Eur. J. Vasc. Endovasc. Surg.* 37, 175 **(2009)**.
11. I. M. Nordon, R. J. Hinchliffe, B. Manning, K. Ivancev, P. J. Holt, I. M. Loftus, and M. M. Thompson, Toward an "off-the-shelf" fenestrated endograft for management of short-necked abdominal aortic aneurysms: An analysis of current graft morphological diversity. *J. Endovasc. Ther.* 17, 78 **(2010)**.
12. Z. Sun, B. P. Mwipatayi, J. B. Semmens, and M. M. Lawrence-Brown, Short to midterm outcomes of fenestrated endovascular grafts in the treatment of abdominal aortic aneurysms: A systematic review. *J. Endovasc. Ther.* 213, 747 **(2006)**.
13. D. S. Zarkowsky, C. W. Hicks, I. C. Bostock, D. H. Stone, M. Eslami, and P. P. Goodney, Renal dysfunction and the associated decrease in survival after elective endovascular aneurysm repair. *J. Vasc. Surg* 64, 1278 **(2016)**.
14. S. C. Paravastu, R. Jayarajasingam, R. Cottam, S. Palfreyman, J. A. Michaels, and S. M. Thomas. Endovascular repair of abdominal aortic aneurysm. *Cochrane. Database. Syst. Rev*. 1, CD004178 **(2014)**.
15. Z. Sun, M. O'Donnell, R. Winder, P. Ellis, and P. Blair, Effect of suprarenal fixation of aortic stent grafts on renal ostium: Assessment of morphological changes by virtual intravascular endoscopy. *J. Endovasc. Ther.* 14, 650 **(2007)**.
16. Z. Sun, Helical CT angiography of abdominal aortic aneurysms treated with suprarenal stent grafting. *Cardiovasc. Intervent. Radiol.* 26, 290 **(2003)**.
17. J. Rydberg, K. K. Kopecky, S. G. Lalka, M. S. Johnson, M. C. Dalsing, and S. A. Persohn, Stent grafting of abdominal aortic aneurysms: Pre- and postoperative evaluation with multislice helical CT. *J. Comput. Assit. Tomgr.* 25, 580 **(2001)**.
18. A. Rozenblit, M. Patlas, A. T. Rosenbaum, T. Okhi, F. J. Veith, M. P. Laks, and Z. J. Ricci, Detection of endoleaks after endovascular repair of abdominal aortic aneurysm repair: Value of unenhanced and delayed helical CT acquisitions. *Radiology* 227, 426 **(2003)**.
19. M. D. Armerding, G. D. Rubin, C. F. Beaulieu, S. M. Slonim, E. W. Samuels, M. J. Jongensen, C. P. Semba, R. B. H. Jeffrey, and M. D. Dake, Aortic aneurysmal disease: Assessment of stent-graft treatment-CT versus conventional angiography. *Radiology.* 215, 138 **(2000)**.
20. S. W. Stavropoulos, T. W. Clark, J. P. Carpenter, R. M. Fairman, H. Litt, O. C. Velazquez, E. Insko, M. Farner, and R. A. Baum, Use of CT angiography to classify endoleaks after endovascular repair of abdominal aortic aneurysms. *J. Vasc. Interv. Radiol.* 16, 663 **(2005)**.
21. Z. Sun, G. H. Choo, and K. H. Ng, Coronary CT angiography: Current status and continuing challenges. *Br. J. Radiol.* 85, 495 **(2012)**.
22. Z. Sun, M. Almoudi, and Y. Cao, CT angiography in the diagnosis of cardiovascular disease: A transformation in cardiovascular CT practice. *Quant. Imaging. Med. Surg.* 4, 376 **(2014)**.
23. S. K. Tan, C. H. Yeong, K. H. Ng, Y. A. Aziz, and Z. Sun, Recent update on radiation dose assessment for the state-of-art coronary computed tomography angiography (CCTA) protocols. *Plos One* 11, e0161543 **(2016)**.
24. Z. Sun and H. Zheng, Cross-sectional area reduction of the renal ostium by suprarenal stent wires: *In vitro* phantom study by CT virtual angioscopy. *Comput. Med. Imaging. Graph.* 28, 345 **(2004)**.
25. Z. Sun, J. Winder, B. Kelly, P. Ellis, P. Kennedy, and D. Hirst, Assessment of VIE image quality using helical CT angiography: *In vitro* phantom study. *Comput. Med. Imaging. Graph.* 28, 3 **(2004)**.
26. Z. Sun and E. Gallagher, Multislice CT virtual intravascular endoscopy for abdominal aortic aneurysm stent grafts. *J. Vasc. Intervent. Radiol.* 15, 961 **(2004)**.
27. Z. Sun and T. Chaichana, Investigation of hemodynamic effect of stent wires on renal arteries in patients with abdominal aortic aneurysms treated with suprarenal stent grafts. *Cardiovasc. Intervent. Radiol.* 32, 647 **(2009)**.
28. K. Liffman, M. D. Lawrence-Brown, J. B. Semmens, I. D. Sutalo, A. Bui, F. White, and D. E. Hartley, Suprarenal fixation: Effect on blood flow of an endoluminal stent wire across an arterial orifice. *J. Endovasc. Ther.* 10, 260 **(2003)**.
29. Z. Sun and T. Chaichana, Fenestrated stent graft repair of abdominal aortic aneurysm: Hemodynamic analysis of effect of fenestrated stents on renal arteries. *Korean. J. Radiol.* 11, 95 **(2010)**.
30. R. Lewis, Medical applications of synchrotron radiation X-rays. *Phys. Med. Biol.* 42, 1213 **(1997)**.
31. Z. Sun, The promise of synchrotron radiation in medical science. *Australasian. Med. J.* 1, 1 **(2009)**.
32. T. Connolley, D. Nash, J. Y. Buffiere, F. Sharif, and P. E. McHugh, X-ray microtomography of a coronary stent deployed in a model artery. *Med. Eng. Phys.* 29, 1132 **(2007)**.
33. W. R. Wix, W. Kupper, T. Dill, C. W. Hamm, H. Job, M. Lohmann, B. Reime, and R. Ventura, Comparison of intravenous coronary angiography using synchrotron radiation with selective coronary angiography. *J. Synchrotron. Radiat.* 10, 219 **(2003)**.
34. Z. Sun and C. Ng, Dual source CT angiography in aortic stent grafting: An *in vitro* aorta phantom study of image noise and radiation dose. *Acad. Radiol.* 17, 884 **(2010)**.
35. P. Thurner, R. Muller, G. Raeber, U, Sennhauser, and J. A. Hubbell, 3D morphology of cell structures: A quantitative approach using micrometer synchrotron light tomography. *Microsc. Res. Tech.* 66, 289 **(2005)**.
36. C. Chappard, F. Peyrin, A. Bonnassie, G. Lemineur, B. Brunet-Imbault, E. Lespessailles, and C. L. Benhamou, Subchondral bone micro-architectural alterations in osteoarthritis: A synchrotron micro-computed tomography study. *Osteoarthritis. Cartilage.* 14, 215 **(2006)**.
37. S. Nuzzo, F. Peyrin, P. Cloetens, J. Baruchel, and G. Boivin, Quantification of the degree of mineralization of bone in three dimensions using synchrotron radiation microtomography. *Med. Phys.* 29, 2672 **(2002)**.

38. O. Betz, U. Wegst, D. Weide, M. Heethoff, L. Helfen, W. K. Lee, and P. Cloetens, Imaging applications of synchrotron X-ray phase-contrast microtomography in biological morphology and biomaterials science. I. General aspects of the technique and its advantages in the analysis of millimeter-size arthropod structure. *J. Microsc.* 227, 51 **(2007)**.

39. S. Winklhofer, S. Peter, F. Morsbach, M. von Werdt, S. Berens, P. Modregger, L. Buser, H. Moch, M. Sampanoni, M. Thali, H. Alkadhi, and P. Stolzmann, Diagnostic accuracy of quantitative and qualitative phase-contrast imaging for the *ex vivo* characterization of human coronary atherosclerotic plaques. *Radiology* 277, 64 **(2015)**.

40. H. Hetterich, M. W. Dipl Phys, S. Fill, J. Herzen, F. Bamberg, A. H. Dipl Phys, U. Schuller, S. Adam-Neumair, S. Wirth, M. Reiser, F. Pfeiffer, and T. Saam, Phase-contrast CT: Qualitative and quantitative evaluation of atherosclerotic carotid artery plaque. *Radiology.* 271, 870 **(2014)**.

41. B. Bertrand, F. Esteve, H. Elleaume, C. Nemoz, S. Fiedler, A. Bravin, G. Berruyer, T. Brochard, M. Renier, J. Machecourt, W. Thomlinson, and J. F. L. Bas, Comparison of synchrotron radiation angiography with conventional angiography for the diagnosis of in-stent restenosis after percutaneous transluminal coronary angioplasty. *Eur. Heart. J.* 26, 1284 **(2015)**.

42. Z. Sun and A. Squelch, Patient-specific 3D printed models of aortic aneurysm and aortic dissection. *J. Med. Imaging. Health. Inf.* 7, 886 **(2017)**.

43. D. Shi, K. Liu, X. Zhang, H. Liao, and X. Chen, Applications of three-dimensional printing technology in the cardiovascular field. *Intern. Emerg. Med.* 10, 759 **(2015)**.

44. A. A. Giannopoulos, M. L. Steigner, E. George, M. Barile, A. R. Hunsaker, F. J. Rybicki, and D. Mitsouras, Cardiothoracic applications of-dimensional printing. *J. Thorac. Imaging* 31, 253 **(2016)**.

Received: 9 September 2016. Accepted: 1 October 2016.